NASA Technical Memorandum 85954

Airborne Astronomy Program
Medium Altitude Missions Branch
Preprint Series 013

NASA-TM-85954 19840018456

NGC 2024: Far-Infrared and Radio Molecular Observations

Harley A. Thronson, Jr.,
Charles J. Lada, P.R. Schwartz,
Howard A. Smith, J. Smith,
W. Glaccum, D.A. Harper,
and R.F. Loewenstein

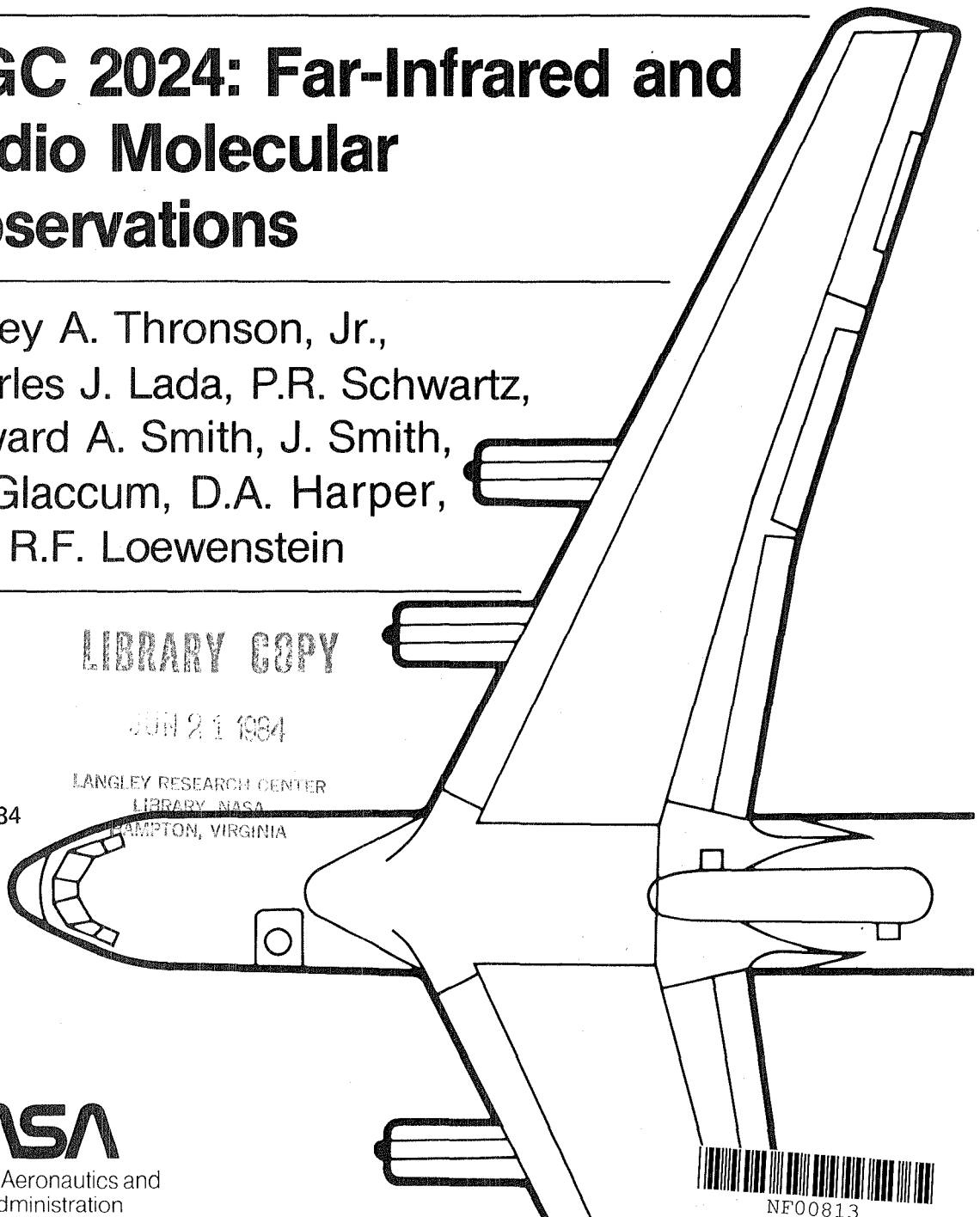May 1984

NASA

National Aeronautics and
Space Administration

NGC 2024: Far-Infrared and Radio Molecular Observations

Harley A. Thronson, Jr., University of Wyoming

Charles J. Lada, University of Arizona

P. R. Schwartz
Howard A. Smith, Naval Research Laboratory, Washington, D. C.

J. Smith, Wyoming Infrared Observatory, University of Wyoming,
         Yerkes Observatory, University of Chicago

W. Glaccum
D. A. Harper
R. F. Loewenstein, Yerkes Observatory, University of Chicago

NASA

National Aeronautics and
Space Administration

Ames Research Center
Moffett Field, California 94035

N84-26524#

NGC 2024:

FAR-INFRARED AND RADIO MOLECULAR

OBSERVATIONS

Harley A Thronson, Jr.,[1], Charles J. Lada[2,3],

P. R. Schwartz[4], Howard A. Smith[4],

and

J. Smith[1,5], W. Glaccum[5], D. A. Harper[5]
and R. F. Loewenstein[5]

[1] Wyoming Infrared Observatory, University of Wyoming

[2] Steward Observatory, University of Arizona

[3] Alfred P. Sloan Foundation Fellow

[4] E.O. Hulburt Center for Space Research, Naval Research Laboratory

[5] Yerkes Observatory, University of Chicago

ABSTRACT

We present new far-infrared continuum and millimeter-wave molecular observations of NGC 2024. The measurements were obtained at relatively high angular resolution, enabling us to describe the source energetics and mass distribution in greater detail than previously reported. The object appears to be dominated by a dense ridge of material, extended in the north-south direction and centered on the dark lane that is seen in visual photographs. Our maps of the source using the "high-density" molecules CS and HCN confirm this picture and allow us to describe the core structure and molecular abundances. The radio molecular and infrared observations support the idea that an important exciting star in NGC 2024 has yet to be identified and is centered on the dense ridge about 1' south of the bright mid-infrared source IRS 2. The data presented here, along with other observations, allow us to describe a model for the source.

Subject headings: infrared: sources -- interstellar:

molecules -- nebulae; H II regions --

nebulae: individual (NGC 2024) --

radio sources: general

I. INTRODUCTION

NGC 2024 (Ori B, W12) is one of the best known infrared and radio sources in the sky. Nevertheless, because of its location close to the Orion Nebula region, it has received less attention than other important objects. Harper (1974) presented the first far-infrared map of the source, obtained at low angular resolution (5'). About the same time Grasdalen (1974) reported detailed near- and mid-infrared observations, discovered a bright infrared point source (IRS 2), and suggested that it was the exciting star for the object. Hudson and Soifer (1976) mapped the object at 400 μm and compared their results with existing far-infrared continuum and millimeter-wave molecular data. Other infrared observations of note are the near-infrared spectroscopy of IRS 1 and IRS 2 by Thompson, Thronson, and Campbell (1981), who investigated the excitation and structure of the source and concluded that the dominant exciting star had yet to be identified. More recently, Black and Willner (1983) discussed high-resolution near-infrared spectroscopy of IRS 2, emphasizing the line-of-sight CO absorption and the nature of the infrared source. In addition Frey et al. (1979) presented near-infrared continuum maps and also argued for multiple sources of excitation.

Detailed high-resolution radio continuum observations of NGC 2024 are not common. An 11 cm map has been presented by Turner et al. (1974), as well as useful single-dish measurements by Rodriguez and Chaisson (1978), Lobert and Goss (1978), Krügel et al. (1982), and Bieging, Wilson, and Downes (1982).

Elaborate radio molecular observations of NGC 2024 are also fairly rare. Bieging, Wilson, and Downes presented H_2CO absorption in the

object and an HCN map credited to Gilmore et al. can be found in Hudson and Soifer. Recently, Snell et al. (1983) reported a detailed investigation of density structure in the object. In addition to this, there are peak antenna temperatures for a number of abundant molecules, but little else.

In this paper we present multi-wavelength far-infrared continuum maps of NGC 2024 at an angular resolution of 49". We also show new $J = 2 \rightarrow 1$ CS and $J = 1 \rightarrow 0$ HCN maps of the source with an angular resolution of 80". These data are combined to discuss the excitation and structure of NGC 2024. In particular, we describe a fairly detailed model to explain the available observations of the object. This source was chosen as it appears we are viewing a shock/ionization front edge-on. Also, the relatively large optical depths in the infrared require that we go to longer wavelengths to study the object. Finally, since the exciting star has never been definitely identified, our multi-wavelength observations give us the opportunity to identify its location.

II. OBSERVATIONS AND METHODS OF ANALYSIS

a.) The Far-infrared Observations

The NGC 2024 region was observed in the far-infrared during a series of flights onboard the NASA Kuiper Airborne Observatory during December, 1981 and January, 1983. The detector system was a multi-filter, seven-element array with an angular resolution of 49" for each detector. The array was made up of a center detector, surrounded by six close-packed detectors. The center-to-center separation for each channel was 55". The reference beam spacing was 8.5 in an east-west direction. Ori A was used for calibration. The object was mapped both by scanning and with position-by-position integrations.

The source was mapped in four filters: three narrow-band filters, having effective wavelengths at 40 μm, 60μm, and 100 μm, and a long-wavelength pass filter with a cut-on at 140 μm. The 100 μm observations were obtained at full-beam spacing, but the other three employed one-half- or one-third-beam spacing, except in the regions of the lowest contours. An area roughly 6' square, centered on the peak of the 60 μm emission, was mapped in all filters, except for the 40 μm filter where an area roughly 4' square was mapped. As will be discussed below, some far-infrared mapping extended further north-south. The results are presented in Fig. 1.

In addition we mapped a cross-shaped region at 200 μm with an 80" beam. This is presented in Fig. 2, superimposed upon a schematic representation of the visual appearance of NGC 2024. We do not have a good calibration for this filter, but we estimate $1.00 = 4 \times 10^3$ Jy in the figure.

The internal uncertainty of our photometry and of the flux density levels in the maps is ± 0.01-0.02 (1σ rms) of the peak. Therefore, the total uncertainty of the quoted flux densities (Table 1 and below) is dominated by external (mainly calibration) uncertainties. From past experience we believe this to be about ± 20%, or less. The absolute positional accuracy of the maps are ± 15" (2σ rms).

Conversion of broadband fluxes to flux densities was accomplished in an iterative manner similar to that described in Thronson and Harper (1979) or Smith et al. (1982). Peak flux densities, as well as the total flux densities, are presented in Table 1. In a 49" beam the peak values are 30-40% larger than those reported by Thronson et al. (1978) at the same resolution. As judged by the maps in Fig. 1, this difference is almost certainly due to the small (2.4) chopper throw used in the earlier observations. The total flux densities in Table 1 are in fair agreement with those of Harper (1974), obtained with a 5' beam. The source spectrum can be represented by an analytic function of the form $F_\nu \propto \nu B_\nu(T)$, where T is taken as a first approximation to the temperature of the dust, T_d, that dominates the far-infrared emission. For positions removed from the peak, the same functional form was assumed to characterize the spectrum, so that T_d could be found from observations made with only two or three filters. The temperature structure in the source is discussed in § III and presented in Fig. 4.

The infrared luminosity (10μm-200μm) of the area mapped in Fig. 1 was 4×10^4 $L_\odot$ at a distance of 0.5 kpc, in agreement with that found by Harper (1974) using a large 5' beam. This is equivalent to the total luminosity of an O9 zero age main sequence (ZAMS) star. As will be discussed below, this luminosity is significantly larger than available from the two well-studied embedded stars (IRS 1 and 2).

b.) The Radio Molecular Observations

Observations of emission from molecules sensitive to high densities were made during January, 1981 using the 11 m telescope of NRAO[6] at Kitt Peak. The 97.98 GHz J = 2 → 1 line of CS was mapped in NGC 2024 at 1' spacings using a 128-channel spectrometer with 100 and 250 kHz

---

[6]The National Radio Astronomy Observatory is operated by Associated Universities, Inc., under contract to the National Science Foundation.

---

resolution. The 88.63 GHz J = 1 → 0 line of HCN was similarly mapped. The angular resolution of the telescope at these two frequencies was about 1.3. Absolute calibration for both objects was obtained primarily by using Ori A, for which we took $T_A^* = 8.4$ K for CS and $T_A^* = 17.2$ K for the J = 1 → 0, F = 2 → 1 line of HCN. Since Ori A was so close in the sky to NGC 2024, corrections for airmass opacity were small. The internal uncertainties in the observations of both molecular species are about 1 σ = 0.3 - 0.5 K for any one position. The pointing uncertainty of the 11m telescope was found to be less than ± 15". The maps of the emission from for both molecular species are presented in Fig. 3a-b as the maximum T_A^* for the line at each position. This should be close to total line strength since the line width did not vary much throughout the source. The velocity structure, as revealed by these high-dipole-moment molecules, is discussed in §IIIb.

One of the goals of this millimeter mapping program was to determine the HCN hyperfine ratios as a function of position in the source. This might then be used as a measure of the variations in

molecular abundances and column densities in the object. In NGC 2024 we found the average hyperfine lines to appear in the ratio 1:0.5:0.2 $[T_A^*(J_F = 1_2 \rightarrow 0_1):T_A^*(J_F=1_1 \rightarrow 0_1): T_A^*(J_F = 1_0 \rightarrow 0_1)]$. This is indistinguishible from the optically thin extreme. The discussion of HCN emission at the molecular peak (§ IIIb) therefore generally applies throughout NGC 2024.

III. DISCUSSION AND ANALYSIS

a.) The Far-Infrared Observations

i. Morphology and Energetics

The far-infrared observations (Fig. 1) show a resolved region of bright emission, extended primarily in the east-west direction at 40 μm, 60 μm and 100 μm, and in contrast, more north-south at 160 μm. Within the uncertainties, the far-infrared peak is coincident with that of the 8.4 μm emission (Grasdalen 1974) and the peak radio molecular emission (discussed more fully in § IIIb). Note also that the higher far-infrared contours encompass the radio continuum peaks (Schraml and Mezger 1969, Turner et al. 1974, Krügel et al. 1982). We therefore suggest that the most likely location for an exciting star is in the general direction of the 60 μm maximum. This position is significantly offset from the two bright near-infrared sources, IRS 1 and IRS 2, which would mean that neither dominates the excitation of the region (see also Balick 1976; Frey et al. 1979; Thompson, Thronson, and Campbell 1981; and Krügel et al.). This picture is further supported by the apparently small effect that the two objects have upon even the lower far-infrared contours and dust temperature (Fig. 4 and next section).

At longer far-infrared wavelengths (Fig. 1d) and at sub-millimeter wavelengths (Hudson and Soifer 1976), the appearance of NGC 2024 changes to a more north-south elongation. This change at the various wavelengths is probably due to the influence of different parameters at the various wavelengths. At far infrared wavelengths between ∿ 40 μm and ∿ 100 μm, for example the emission depends very sensitively upon temperature, but only modestly upon emission optical depth (i.e., column density of warm dust). Longer wavelengths --- $\gtrsim 150\,\mu m$ -- are usually

on the Rayleigh-Jeans side of the source spectrum, and the emission is much less sensitive to variations in dust temperature. Column density variations therefore become proportionately more influential. Model infrared sources show this effect clearly (e.g., Leung 1976, Natta and Panagia 1976; Rowan-Robinson 1979, 1980). On the basis of our observations then, NGC 2024 is dominated by a warm high column density ridge, elongated primarily in the north-south direction, toward which are found the exciting stars. Unfortunately our 200 μm observations are not complete enough to confirm this north-south extent.

The total far-infrared luminosity of the NGC 2024 infrared source is close to that of an O9 ZAMS star, or an ensemble of stars of equivalent luminosity. The same conclusion was reached by calculating the ionizing flux necessary to power the radio continuum source (Krügel et al. 1982). This suggests that there is very little dust mixed with the ionized gas in the source, which is usually the case for H II regions of only low to moderate densities (i.e., $n_H \lesssim 10^4$ cm^{-3}). The compact or ultra-compact H II regions, on the other hand, almost invariably appear to have dust within the ionized zone, resulting in a significant reduction of the ionizing flux (e.g., Thronson and Harper 1979; Habing and Israel 1979). The identification of a late O/early B star as the ultimate power source is also in agreement with the low He/H ratio derived from radio recombination lines (Cesarsky 1977, Churchwell et al. 1978, Krügel et al.).

If IRS 2 is a B0.5 ZAMS star, as suggested by Thompson, Thronson, and Campbell (1981), it should make no more than about a 20% contribution to the total luminosity and ionizing flux of the region. This is consistent with our conclusions drawn from the appearance of the

maps in Fig. 1. Since IRS 1 was classified B0.5 V by Johnson and Mendoza (1964), similar considerations apply. It is therefore not surprising that some of the radio continuum maps referenced above show modest extension in the direction of IRS 1. However, with these two objects making up at most roughly 40% of the total excitation, an additional energy source with a luminosity equivalent to about a B0 ZAMS star remains to be found.

An interesting feature that appears on both the 60 μm and the 160 μm maps is a knot of emission about 4' north of the far-infrared peak (the 100 μm and 40 μm maps did not extend far enough north). The "high-density" molecular emission (§ III b) also seems to show a feature in this region. There is nothing prominent at this position in the very red photograph of Grasdalen (1974). The total far-infrared luminosity in a 49" beam at the position of this small feature is about 400 $L_{\odot}$, giving a good idea of the limiting sensitivity in our observations.

11. Dust Temperature

The observations at 60 μm and 160 μm were used to determine the dust temperature, since these two filters had the most extensive spatial coverage and generally the highest signal-to-noise. The results are presented in Fig. 4. As with most far-infrared sources, the changes in T_d over the source are fairly gradual. This is a simple reflection of the very weak dependence of dust temperature upon the more significant source parameters: geometry, radiation field, and grain composition. We note that the dust temperature at, or close to, the radio molecular maximum is only several degrees above that deduced for the gas using several methods ($T_g \sim$ 40-45 K; Plambeck and Williams 1979, Loren et al.

1981, Black and Willner 1983). This is consistent with gas heating via thermal coupling with the dust under conditions of at least modestly high densities ($n_{H_2} \gtrsim 10^5 \, cm^{-3}$, from the results of Goldsmith and Langer 1978; see also Snell et al. 1983).

Only directly south of the peak does T_d change rapidly. One arcmin south, $T_d \sim 35$ K, and two arcmin south, $T_d \sim 25$ K. By contrast, $T_d \sim 40$ K as far as two arcmin north of the peak. East and west of the central position, T_d changes only very little, by a few degrees. IRS 1 and IRS 2 may contribute to the maintaining of high temperature in these directions. There is a hot spot 1½ arcmin to the east of the flux density peak where $T_d = 58$ K, but all the points surrounding this position are around 53 K. The most striking feature of Fig. 4 is therefore the very abrupt drop in dust temperature directly south of the 60 μm maximum. Emission at the shorter wavelengths of Fig. 1, particularly at 40 μm, are well on the Wien side of the dust emission in this region. The emission is quite weak, compared to the rest of the source and the object therefore appears broader in the east-west direction.

This temperature distribution is characteristic of exciting stars that are abutting a very dense molecular cloud at which we are looking in cross-section. In the case of NGC 2024 a dense part of the cloud lies just to the south of the infrared and radio continuum peaks. Rapid absorption of photons causes the dust temperature to drop very sharply over a distance of only one arcminute. Elsewhere the temperature gradient is quite gentle, which suggests that any extinction of photons in other directions is more modest.

This general description is supported by radio continuum observations (Krügel et al.; J. Bieging, private communication) which show very steep contours at the south edge of the H II region. Here the ionizing photons are being very suddenly absorbed.

Our interpretation of the dust temperature map is in agreement with the 8.7 μm map presented by Grasdalen. Its maximum is 1' south of IRS 2 and the emission is elongated east-west. Because mid-infrared emission should show the distribution of the hottest material, it is reasonable that the dominant exciting stars are close to the position of the 8.7 μm maximum.

iii. Far-infrared Optical Depth

With a temperature known, the 60 μm emission optical depth (τ_{60}) can be found from the flux density using $F_{\nu} = \tau_{60} B_{\nu}(T_d) \Omega$, where Ω is the beam solid angle. The 60 μm optical depth was thereby mapped in NGC 2024 and is presented in Fig. 5. Much of the discussion in the preceding two sections can now be quantified. At far-infrared wavelengths NGC 2024 is very bright, which implies that the emission optical depth is large. Using the method described in § IIa we found the 60 μm optical depth to be $\tau_{60} = 0.3$ at the peak. Due to the simplifying assumptions necessary for the calculation, this value is probably uncertain by a factor of at least 3. Nevertheless, a high optical depth is also supported by observations (Lemke and Low 1972) that suggest optically thick mid-infrared emission and by an optical depth at 400 μm (Hudson and Soifer 1976) in agreement with that found here, if extrapolated using reasonable assumptions.

This is fairly high for an optical depth at 60 μm, and is matched by similarly high values throughout the rest of the cloud. Fig. 5 is a contour map of τ_{60}, each point calculated as for the peak. Although the

uncertainty in the absolute values for τ_{60} is large, the <u>relative</u> uncertainties are much lower and the figure should be a good representation of the distribution of far-infrared-emitting dust. It is not unusual to find the maximum optical depth toward the location of the exciting stars. However, this maximum does not fall off rapidly in either the north or south direction. The figure graphically shows that the core of NGC 2024 is dominated by an extended high-column-density ridge. This north-south extent is consistent with the visual appearance of NGC 2024 (c.f., Grasdalen, 1974, Balick 1976, Fig. 2). This morphology was predicted by the behavior of $160 \, \mu m$ emission which was more heavily influenced by the column density of dust than was emission at shorter wavelengths.

The far-infrared optical depth can be converted to a visual extinction, since $\tau_{60} \sim 0.003 \, A_V$ (Gatley <u>et al.</u> 1977; Rowan-Robinson 1979; Keene 1981). Therefore, $A_V \sim 100$ mag at the far-infrared peak, dropping to $A_V \sim 15$ mags at the outer edges of the core. It is worth emphasizing that the far-infrared optical depth contours do not show any significant effect due to the presence of IRS 1 or 2.

On the basis of molecular observations discussed in the following sections, we are going to argue that the bulk of the dust is foreground to the ionized gas and exciting stars. In the direction of IRS 2, our far-infrared optical depth suggests a visual extinction close to 50 mags. For this object Thompson, Thronson, and Campbell (1981) found only $A_V = 12 \pm 3$ mags from the Brackett line series. Although there are significant systematic uncertainties in τ_{60}, we consider this difference to be real and suggest that IRS 2 is buried only part way into the NGC 2024 cloud as we view it from Earth. Under these conditions it appears

brighter in the near-infrared than would more luminous stars located at the far-infrared/radio continuum peak and would thereby attract more attention. For example, on the basis of Fig. 5, a B0.5 ZAMS star like IRS 2 (Thompson et al.) would appear 8 magnitudes fainter at [K] if moved to the center of the H II region and behind the far-infrared-emitting dust.

The various observations of NGC 2024 allow a calculation of the mass of the molecular cloud mapped here. A number of authors have derived relations between molecular column density and far-infrared optical depth (c.f., Evans, Blair, and Beckwith 1977; Righini-Cohen and Simon 1977; Sargent et al. 1981; Keene, Hildebrand, and Whitcomb 1982; Thronson et al. 1983; §IIIbii). Because of the similarity of assumptions, we adopt the relation found by Thronson et al., $\tau_{60} = 6 \times 10^{-19} N(^{13}CO)$; except for the results in Righini-Cohen and Simon, the other studies give similar values. Therefore, toward the center of NGC 2024, $N(^{13}CO) \sim 5 \times 10^{17}$ cm^{-2}, or $N(H_2) \sim 2 \times 10^{23}$, if $[^{13}CO]/[H_2] = 3 \times 10^{-6}$ (see also Black and Willner [1983] and §IIIbii). The same data may be used to estimate the total mass of the region mapped in the far-infrared. Integrating over Fig. 5 we get $M_H \sim 500 M_\odot$. Averaged over the region mapped in HCN and CS emission (Fig. 3) this translates into densities in the range of a few times 10^5 cm^{-3}. This mass estimate agrees with the virial mass derived by Snell et al. and supports the hypothesis of dense clumps within a more tenuous gas. The more detailed analysis of densities by Snell et al. estimate about an order of magnitude greater values than we do here. This probably reflects the fact that their CS data is weighted toward higher densities.

b.) The Millimeter-Wave Observations

i. Morphology and Velocity Structure

Most of the far-infrared emission observed from regions of star formation usually arises from the denser, central regions of an object. On the basis of the preceding discussion, this appears to be the case for NGC 2024. For this reason we have mapped the central regions of the source in the emission from HCN and CS (Fig. 3). Both molecules have relatively high dipole moments and are therefore excited under conditions of high density. Emission from HCN is typically seen where $n_H \gtrsim 3 \times 10^4$ cm^{-3} (e.g., Gottlieb et al. 1975) and J = 2 → 1 CS is found where $n_{H_2} \gtrsim 10^5$ cm^{-3} (e.g., Linke and Goldsmith 1980, Snell et al.). Although superior in signal-to-noise, our HCN map is in good agreement with that of Gilmore et al. (1975, see Hudson and Soifer 1976). Likewise, our CS map is in agreement with, but of superior quality, to that of Snell et al.

Both species show a peak in T_A^* close to the location of the far-infrared and radio continuum peaks. The emission is generally elongated in the north-south direction, co-extensive with the dark bar in NGC 2024, the sub-millimeter emission, and the 60 μm optical depth distribution. The extent of emission and the fact that the molecules are excited by high densities also confirm the high extinction derived for the center of the cloud. They extend the far-infrared picture in important ways as well.

Fig. 5 shows the column density of warm dust and presumably the associated gas. Although the molecular emission can be affected by temperature and radiative transfer (optical depth) effects, the distribution of CS or HCN emission is a good indicator of the high

volume density distribution. Therefore Fig. 3 suggests that the high column density ridge in Fig. 5 is due mainly to a high volume density. The core of NGC 2024 is dominated by a dense, centrally-located, cylinder-like region.

The preceding discussion includes at least two significant provisos. The first is the role of optical depth in molecular emission. Models (Gottlieb et al.1975; Kwan and Scoville 1975) suggest that the emission from HCN is more susceptible to complicated radiative transfer effects than is the CS emission. Quantitative estimates of this effect presumably await detailed observations of higher level transitions, but it seems a resonable explanation for the apparent differences in structure between Figs. 3a and 3b.

An additional consideration that probably affects the CS molecule more is that of radiative excitation. This is probably a minor consideration in NGC 2024 since the source is so extended and of only modest luminosity. This effect has been considered for NGC 2024 by Snell et al.

The velocity distribution in NGC 2024 shows a very interesting structure. Here we consider the V_{LSR} at the line maximum of the $J = 1 \rightarrow 0$, $F = 2 \rightarrow 1$ line of HCN, since it was usually observed at higher spectral resolution (0.33 km s^{-1}) than was CS. As with all strong radio molecular emission observed from NGC 2024 (e.g., Thompson, Thronson, and Campbell 1981), the line center V_{LSR} is within 1 km s^{-1} of +10 km s^{-1} throughout the region mapped. However, just as a central ridge has been revealed by column and volume density tracers, so does the HCN velocity show a characteristic ridge. A north-south cut through the peak of NGC 2024 --- along the high-density core --- has $V_{LSR} = 10.5 \pm 0.2$ km s^{-1}.

There is no evidence for a north-to-south gradient greater than about 0.3 km s^{-1} over the region mapped. However, one angular resolution element either to the west or east of this ridge, V_{LSR} = 10.0 ± 0.2 km s^{-1}. Another resolution element in either direction and there is a further decrease to V_{LSR} = 9.5 ± 0.3 km s^{-1}. The central ridge therefore appears to be moving away from the surrounding parts of the cloud at $\sim$ 1 km s^{-1}.

The high-density velocity structure should be compared with that found for other components in NGC 2024 as this will be important evidence for the model described in the following section. There appear to be two velocity components in the object. As already noted, all strong molecular emission and absorption have V_{LSR} = 9-10 km s^{-1} (Thompson, Thronson, and Campbell; Bieging et al. 1982). This velocity is also close to that of the strongest H I absorption (Lockhart and Goss 1978) and C II emission (Wilson et al. 1975, Krügel et al. 1982). However, the strongest ionized H and He emission is found at 5-7 km s^{-1} (Krügel et al.), along with weaker CO emission. Since different velocities may refer to different locations in space, these observations bear directly upon the structure of NGC 2024.

II. Molecular Abundances and Column Densities

Certain useful relations can be derived using the improved radio and infrared data presented here as well as results from the literature. We are first interested in estimating the column densities of the two molecules observed here and comparing the result with the 60 μm emission optical depth. The following analysis implicitly assumes that the far-infrared emission is co-extensive with that of the molecules.

Detailed radiative transfer and statistical equilibrium models are required to fully analyze the HCN and CS emission (e.g., Snell et al.). Because we are satisfied with order-of-magnitude estimates, we shall instead adopt the assumption of thermodynamic equilibrium so that the molecular column density may be specified by a single excitation temperature. For CS we use

$$N(CS) = \frac{1.9 \times 10^{12} \tau_{CS} T_{ex}(CS) \Delta v}{1 - \exp(-7.1/T_{ex}(CS))} ,$$

where τ_{CS} is the optical depth of the $J = 2 \rightarrow 1$ line, T_{ex} is the molecule's excitation temperature, and Δv is the linewidth in NGC 2024 (3.5 km s^{-1}). Under the fairly high density conditions of the core of NGC 2024, it is likely that $T_{ex}(CS) \sim T_k = 45$ K and that $\tau_{CS} \rightarrow 1$. In any case, these particular values serve as upper limits for the above equation. We therefore estimate $N(CS) \leq 2 \times 10^{15}$ cm^{-2}; hence, $N(CS) \leq 6 \times 10^{15} \tau_{60}$ cm^{-2}. Snell et al. (1983) estimated the CS column density in NGC 2024 using a multi-level model. They calculated $N(CS) = 1.6 \times 10^{14}$ cm^{-2} toward the infrared/molecular maximum. This result gives $N(CS) = 5 \times 10^{14} \tau_{60}$, in agreement with the limit from our data.

The HCN molecule is more difficult to analyze ———— even in the simple manner adopted here ———— because of significant ambiguities in the transfer of its radiation through a dense molecular cloud. Gottlieb et al. (1975) were able to fit observed HCN hyperfine line ratios with a farily straightforward model of optically-thin emission. Kwan and Scoville (1975) argue instead that significant radiation trapping can alter the molecule's level populations and thereby duplicate the appearance of optically-thin emission. However, we note that in the

case of NGC 2024, $T_A^*(HCN) \ll T_K$, as shown in Fig. 3b. According to the models of Kwan and Scoville, the emission therefore has only modest optical depth under the high density conditions calculated for this object. Under these circumstances we can use the Gottlieb et al. calculations to estimate the HCN column density. At the far-infrared peak we have $T_A^*(J_F = 1_2 \rightarrow 0_1) = 7$ K, $T_A^*(J_F = 1_0 \rightarrow 0_1) = 1.5$ K, and $T_A^*(J_F = 1_1 \rightarrow 0_1) = 3.1$ K. On the basis of the velocity structure described in the previous section, we shall take $dv/dr = 1$ km s^{-1} pc^{-1}. From Gottlieb et al., therefore, we estimate $N(HCN) = 1 \times 10^{13}$ cm^{-2}, where we used $n_{H_2} = 1.6 \times 10^6$ cm^{-3} from Snell et al.. This gives $N(HCN) = 3 \times 10^{13} \tau_{60}^2$ cm^{-2}.

Column densities have been calculated for a number of other species toward the NGC 2024. In particular, Goss et al. (1976) calculated the OH abundance, Lockhart and Goss (1978) found the H I absorption, Genzel et al. (1979) estimated both CH and H_2CO column densities, Hollis and Churchwell (1983) studied HCO, and Black and Willner (1983) estimated the amount of H_2 and CO in front of IRS 2. All of these values, and those we estimated for HCN and CS, are collected in Table 2 where we present the ratio of column density to $60 \mu m$ optical depth. Where the beam size of the radio observation significantly exceeded that of the far-infrared data ———— or where it referred to a position other than the peak ———— corrections were made to the infrared optical depth.

We emphasize again that the combined uncertainties of the radio and far-infrared data mean that Table 2 can only be an order-of-magnitude tabulation. It is therefore not surprising that the relative abundances in NGC 2024, as well as the ratios of molecular column densities to dust optical depth, are in general agreement with other work (e.g., the $N(CO)/\tau_{IR}$ relations in Thronson et al. 1983).

c.) A Model

The observations presented here and elsewhere allow a model of NGC 2024 to be created. We first summarize our findings.

NGC 2024 is dominated by a high density core elongated in the north-south direction. The column density through the center of the cloud is equivalent to roughly 100 visual magnitudes of extinction. The peak in far-infrared emission is coincident with the maximum antenna temperature of CS and HCN, and close to the radio continuum maximum. The two bright near-infrared sources - IRS 1 and IRS 2 -probably combine to contribute less than about half of the total far-infrared luminosity of the source. An additional exciting star awaits discovery and is most likely located toward the radio/infrared maximum.

In many respects our description of NGC 2024 is in agreement with the model suggested by Krügel et al. (see their Fig. 7). The H II region lies behind the dense molecular cloud, as demonstrated by the H_2CO absorption studies (Bieging et al. 1982). The cause of the two velocity components is the acceleration of ionized gas away from a cavity in the cloud and in a direction somewhat toward the observer.

Our modification to the Krügel et al. model is as follows. First, as already noted, we find no evidence for IRS 2 playing a major role in source excitation and we believe that this object is most likely embedded partway into the cloud core, as viewed from Earth (Krügel et al. were unable to satisfactorily determine the role of IRS 2 in the source.). Second, there seems to be very little evidence for a significant amount of molecular material on the backside (as viewed from Earth) of the H II region, except as might be necessary to confine the ionized gas. Visual photographs and radio continuum observations

suggest that behind the dark bar lies a diffuse - not compact - H II region, and our preference is therefore to minimize the amount of molecular material that completely surrounds it.

On the basis of Fig. 2 we also suggest that much of the <u>visually</u> bright material seen in NGC 2024 lies forward of the bulk of the molecular material as viewed from earth. Our 200 μm map extends into the region of strong visual emission, but it shows no rapid decrease at these positions. This means that the dust (and gas) likewise does not decrease rapidly. This is difficult to quantity, however, since we have no dust temperature information in the outer parts of the cloud.

We note that this picture of NGC 2024 is qualitatively similar to that of the M42/BN-KL region, if the latter was turned 180° away from our line of sight. We suggest that if we were to view NGC 2024 from its backside we would see a visually bright, diffuse H II region, excited by a centrally located BO ZAMS star. Behind this ionized zone would lie a very dense molecular cloud, within which is embedded a lower luminosity object (IRS 2), offset $\sim$ 1' from the most luminous star. Except for differences in luminosity, and perhaps evolutionary stage, this is what is found in M42.

ADDRESSES

W. Glaccum, D. Harper, and R. Loewenstein

   Yerkes Observatory

   Williams Bay, WI   53191

C. J. Lada

   Steward Observatory

   University of Arizona

   Tucson, Arizona 85721

P. R. Schwartz and H. A. Smith

   E. O. Hulbert Center for Space Research

   Naval Research Laboratory

   Washington, D.C.   20375

J. Smith and H. Thronson

   Department of Physics and Astronomy

   University of Wyoming

   Laramie, WY   82071

TABLE 1

Source Parameters

Far-infrared Peak Position

$\alpha(1950) = 5^h\ 39^m\ 13^s \pm 1^s$

$\delta(1950) = -1° \ 57' \ 0'' \ \pm 15''$

Flux Density

	Peak (49" Beam)	TOTAL
40μm	8200 Jy	33,000 Jy
60μm	12,000	74,000
100μm	12,000	85,000
160μm	5,700	47,000

Dust Temperature at Peak	48 ± 7 K
Optical Depth at Peak (60μm)	0.3
Infrared Luminosity (10-200μm; 500 pc)	$4 \times 10^4\ L_\odot$
Mass of Molecular Cloud Core	$500\ M_\odot$

TABLE 2

Column Densities vs 60μm Optical Depth

X	$N(X)/\tau_{60}$	References for $N(X)$
H_2	$\leq 4 \times 10^{23}$	1
H	7×10^{21}	2
^{12}CO	$3-9 \times 10^{19}$	1,3
CS	5×10^{14}	4,5
HCN	3×10^{13}	5
OH	9×10^{15}	6
H_2CO	9×10^{13}	7
CH	2×10^{14}	7
HCO	$2-4 \times 10^{13}$	8

[1] Black and Willner (1983)

[2] Lockhart and Goss (1978)

[3] Wilson et al. (1974)

[4] Snell et al. (1983)

[5] This work, § III bii

[6] Goss et al. (1976); very large beam

[7] Genzel et al. (1979)

[8] Hollis and Churchwell (1983)

REFERENCES

Balick, B. 1976, Ap. J., 208, 75.

Bieging, J. H., Wilson, T. L., and Downes, D. 1982, Astr. Ap. Suppl., 49, 607.

Black, J. H., and Willner, S. P. 1983, preprint submitted to Ap. J.

Cesarsky, D. A. 1977, Astr. Ap., 54, 765.

Churchwell, E., Smith, L. F., Mathis, J., Mezger, P. G., Huchtmeier,
    W. 1978, Astr. Ap., 70, 719.

Evans, N. J., Blair, G. N., and Beckwith, S. 1977, Ap. J., 217, 448.

Frey, A., Lemke, D., Thum, C., and Fahrback, U. 1979, Astr. Ap., 74, 133.

Gatley, I., Becklin, E., Werner, M., and Wynn-Williams, C. G. 1977,
    Ap. J., 216, 277.

Genzel, R., Downes, D., Pauls, T., Wilson, T. L., and Bieging, J. 1979,
    Astr. Ap., 73, 253.

Goldsmith, P. F., and Langer, W. D. 1978, Ap. J., 222, 881.

Goss, W. M., Winnberg, A., Johansson, L. E. B., and Fournier, A. 1976,
    Astr. Ap., 46, 1.

Gottlieb, C. A., Lada, C. J., Gottlieb, E. W., Lilley, A. E., and Litvak,
    M. M. 1975, Ap. J., 202, 655.

Grasdalen, G. L. 1974, Ap. J., 193, 373.

Habing, H. J., and Israel, F. P. 1979, Ann. Rev. Astr. Ap., 17, 345.

Harper, D. A. 1974, Ap. J., 192, 557.

Hollis, J. M., and Churchwell, E. 1983, Ap. J., 271, 170.

Hudson, H., and Soifer, B. 1976, Ap. J., 206, 100.

Johnson, H. L., and Mendoza, E. E. 1964, Bol. Obs. Tonantzitla y Tacubaya,
    3, 331.

Keene, J., Hildebrand, R., and Whitcomb, S. 1982, Ap. J. (Letters), 252, L11.

Keene, J. 1981, Ap. J., 245, 115.

Krügel, E., Thum, C., Martin-Pitado, J., and Pankonin. V. 1982, Astr. Ap.
    Suppl, 48, 345.

Kwan, J., and Scoville, N. 1975, Ap. J.(Letters), 195, L85.

Leung, C. M. 1976, Ap. J., 209, 75.

Lemke, D., and Low, F. 1972, Ap. J. (Letters), 177, L53.

Lobert, W., and Goss, W. M. 1978, M.N.R.A.S., 183, 119.

Linke, R. A., and Goldsmith, R. F. 1980, Ap. J., 235, 437.

Lockhart, and Goss 1978, Astr. Ap., 67, 355.

Loren, R. B., Plambeck, R. L., Davis, J. H., and Snell, R. L. 1981, Ap. J.
    245, 495.

Natta, A., and Panagia, N. 1976, Astr. Ap., 50, 191.

Plambeck, R. L., and WIlliams, D. R. W. 1979, Ap. J. (Letters),
    227, L43.

Righini-Cohen, G., and Simon, M. 1977, Ap. J., 213 390.

Rodriguez, L., and Chaisson, E. 1978, Ap. J. 221, 816.

Rowan-Robinson, M. 1979, Ap. J., 234, 111.

Rowan-Robinson, M. 1980, Ap. J. Supp., 44, 403.

Sargent, A. I., van Duinen, R. J., Fridlund, C. V., Nordh, H. L.,
    and Aalders, J. W. 1981, Ap. J., 249, 607.

Schraml, J., and Mezger, P. 1969, Ap. J., 156, 269.

Smith, H. A., Thronson, H. A., Lada, C. J., Harper, D. A., Loewenstein, R. F.,
    and Smith, J. 1982, Ap. J., 258, 170.

Snell, R. L., Mundy, L. G., Goldmsith, P. F., Evans, N. J., and
    Erickson, N. R. 1983, preprint.

Thompson, R. I., Thronson, H. A., and Campbell, B. G. 1981, Ap. J., 249, 622.

Thronson, H. A., and Harper, D. A. 1979, Ap. J., 230, 133.

Thronson, H. A., Harper, D. A., Keene, J., Loewenstein, R. F., Moseley, S. H., and Telesco, C. M. 1978, Ap. J., 83, 492.

Thronson, H. A., Smith, H. A., Lada, C. J., Glaccum, W., Harper. D. A., Loewenstein, R. F., and Smith, J. 1983, MNRAS, in press.

Turner, B. E., Balick, B., Cudaback, D., Heiles, C., and Boyle, R. 1974, Ap. J., 194, 279.

Wilson, W. J., et al. 1974, Ap. J., 191, 357.

FIGURE CAPTIONS

Fig. 1a-d - The flux density distribution in NGC 2024 in four far-infrared passbands. The contours are normalized to 1.00 at the peak. The lowest contour level was chosen to approximately encompass the extent of the mapped region; the dashed lines are extrapolations. A typical 1σ uncertainty is 0.01-0.02 of the peak (internal errors only). The small cross in the center of each map is the location of the 60 µm peak. The larger cross above this is the location of IRS 2. The cross in the west side of the figure is the location of IRS 1. The arms of these latter two crosses are each 15" long, the estimated 2σ uncertainty in absolute position of the far-infrared observations.

Fig. 2 - The 200 µm flux density mapped in a cross-shaped pattern in NGC 2024. The location and beam size of the observations are represented as circles. The normalization of the flux density is to 1.00 at the peak. The extent of the visual emission from the source is shown as a cross-hatched distribution. The three crosses have the same meaning as in Fig. 1.

Fig. 3a-b - The corrected antenna temperature distribution for CS and HCN in NGC 2024. The contours are in Kelvins and the lowest contour was chosen to approximately encompass the extent of the mapped region; dashed lines are extrapolations. A typical 1σ uncertainty is 0.3-0.5 K for both molecules. The three crosses have the same meaning as in Fig. 1.

Fig. 4 - The dust temperature distribution, determined from our 60 μm and 160 μm observations as described in the text. The dashed lines are extrapolations and the crosses have the same meaning as in Fig. 1.

Fig. 5 - The 60 μm emission optical depth in NGC 2024. The values were calculated as described in the text. The dashed lines are extrapolations. The crosses have the same meaning as in Fig. 1.
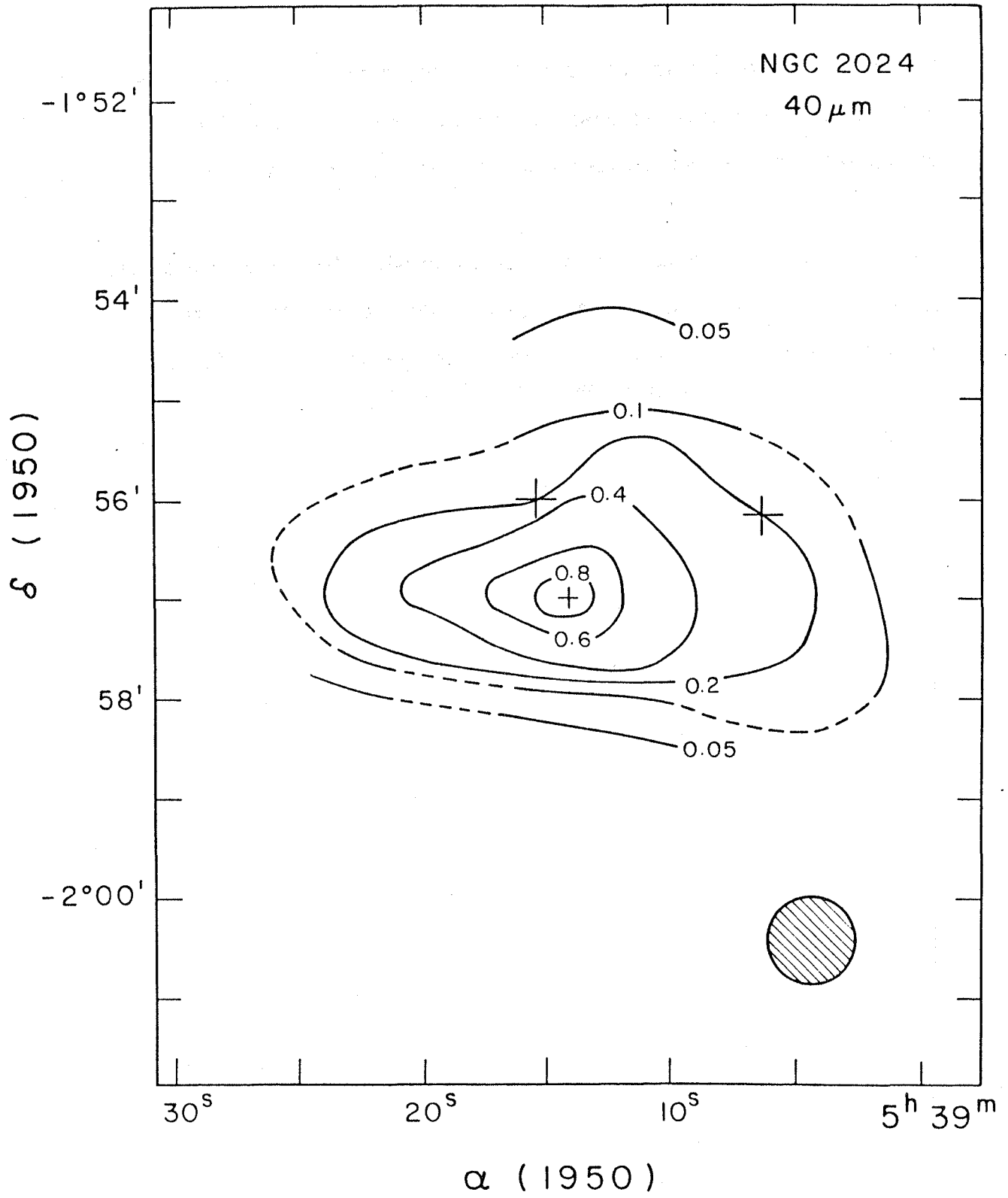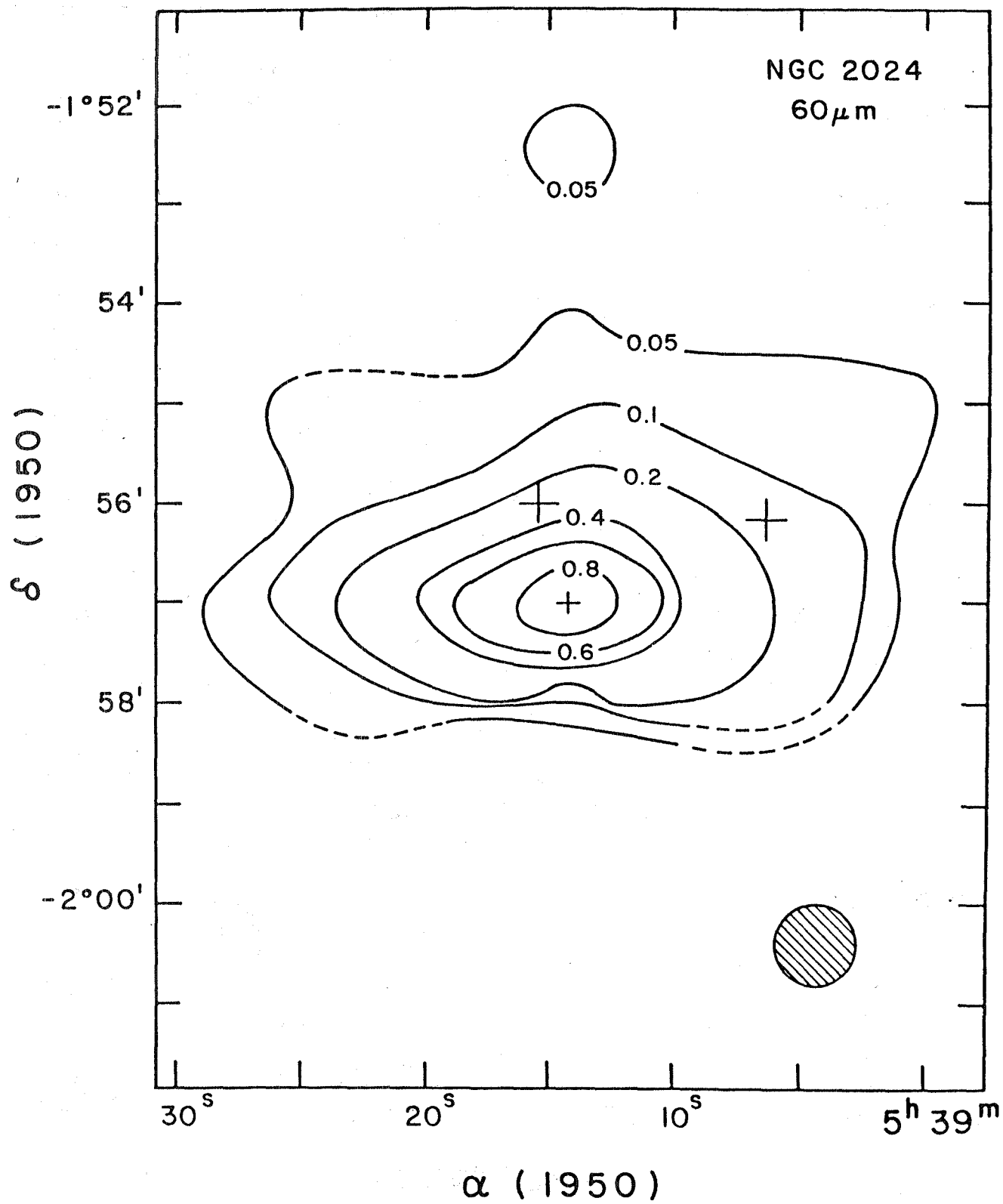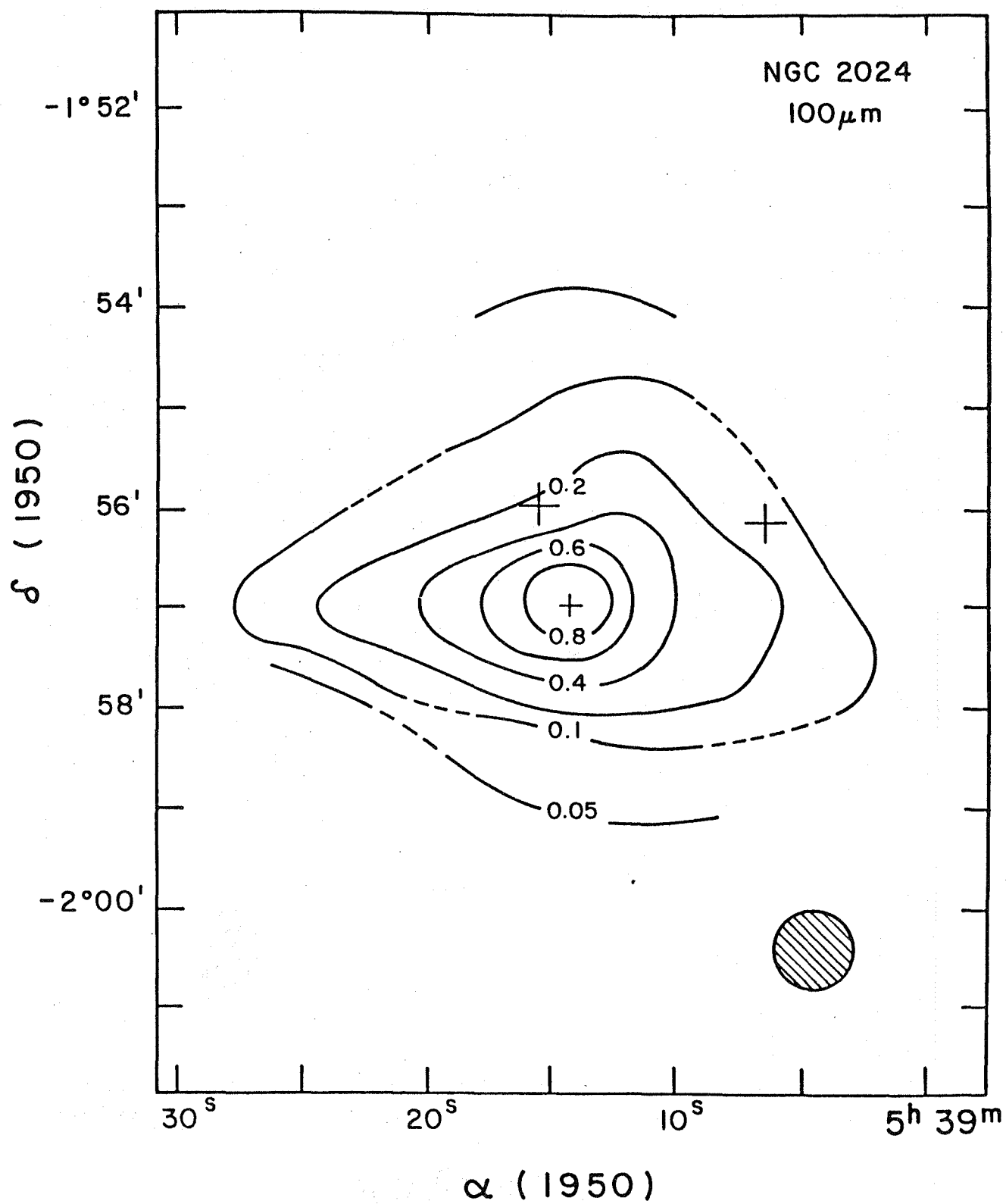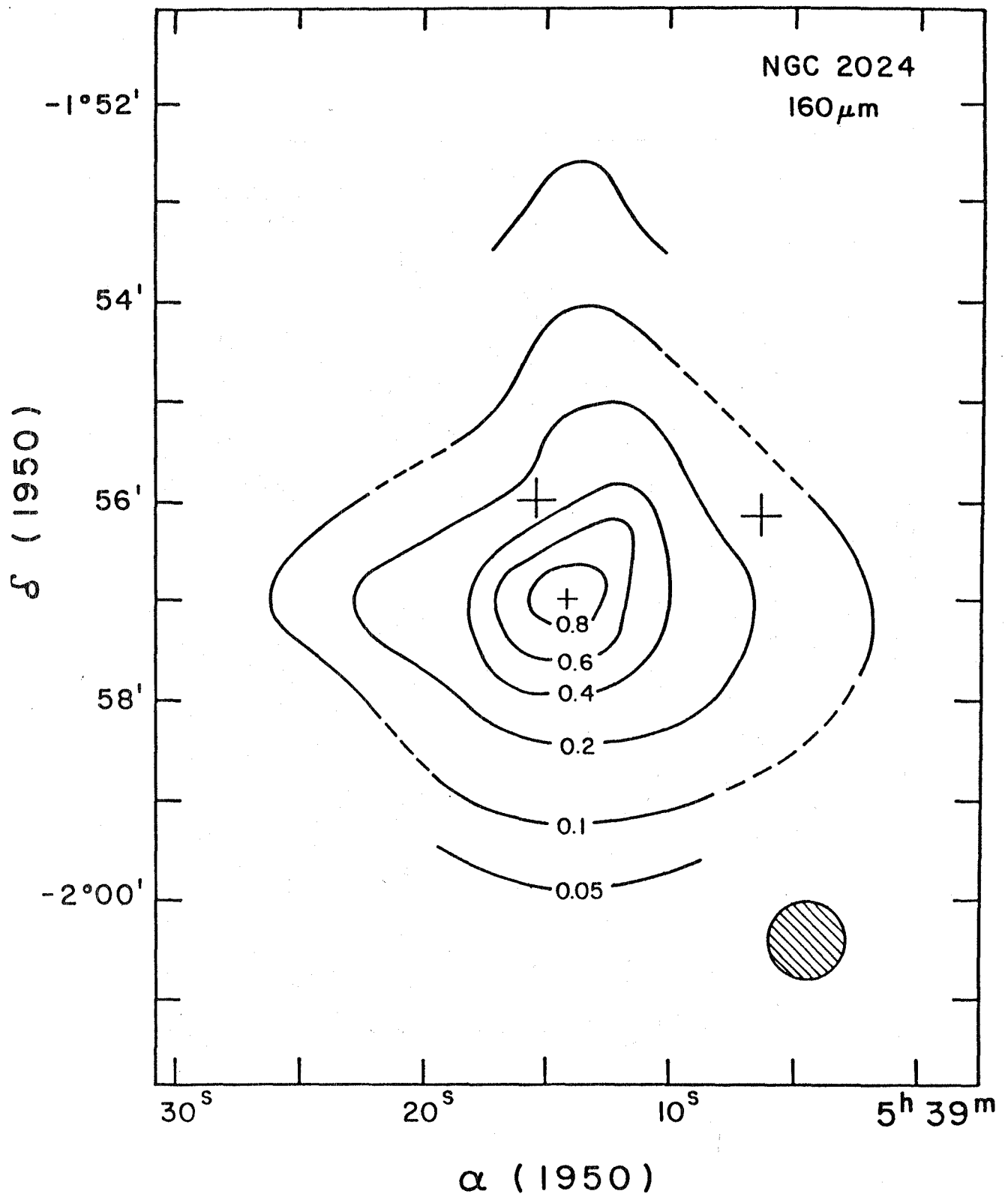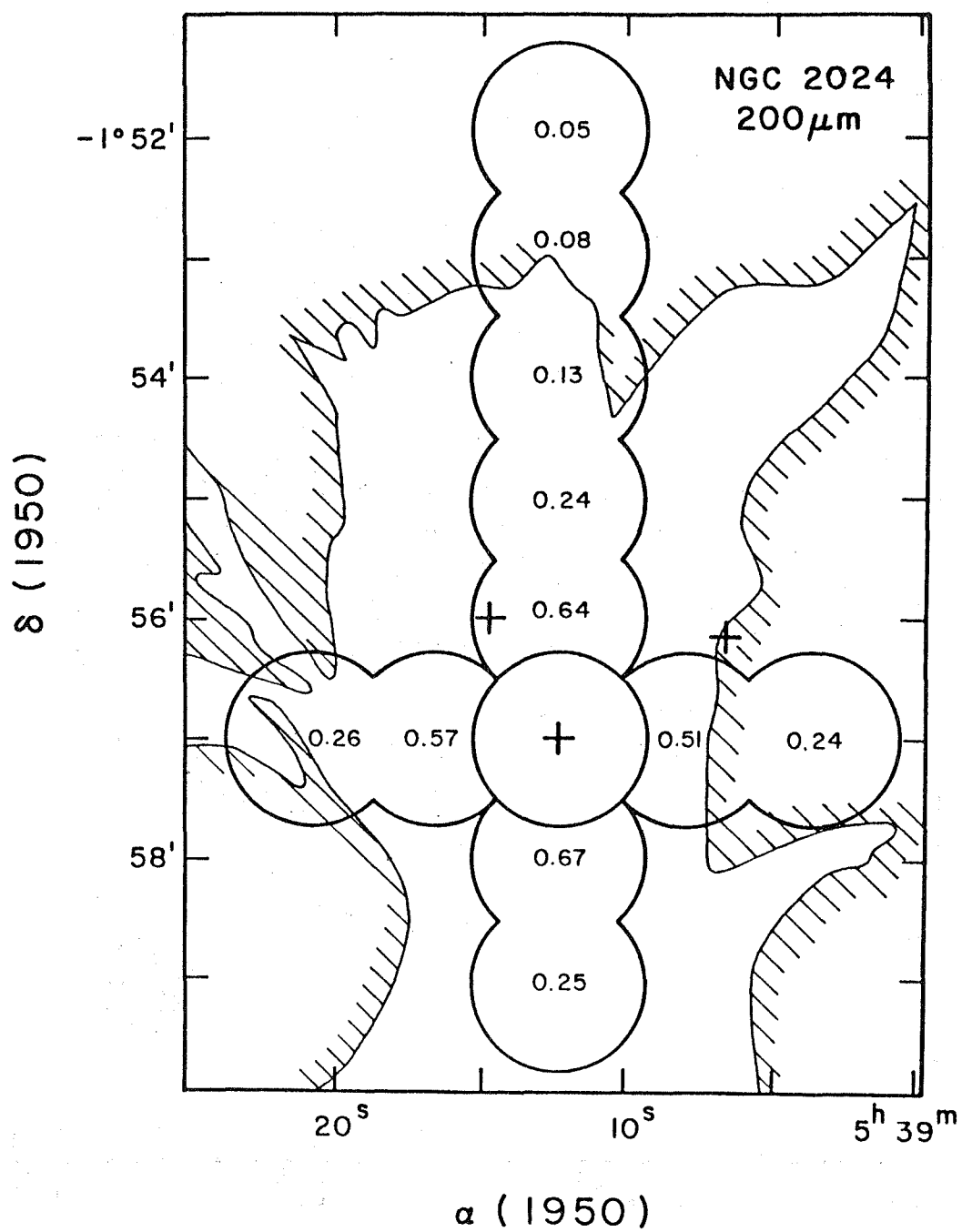
NGC 2024
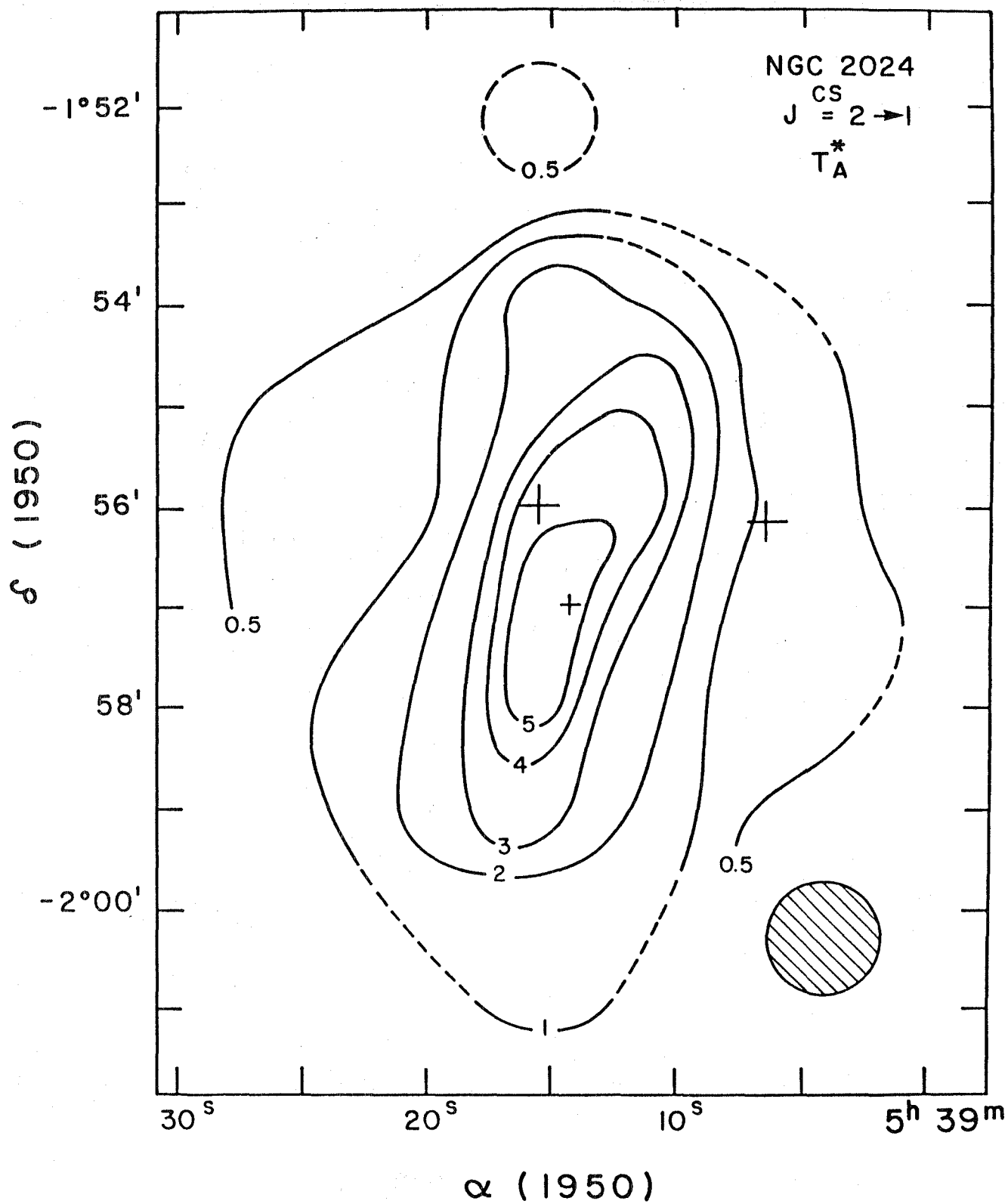40 μm

Fig. 1

Fig. 2

Fig. 3

Fig. 4

Fig. 5

Fig. 6

Fig. 7
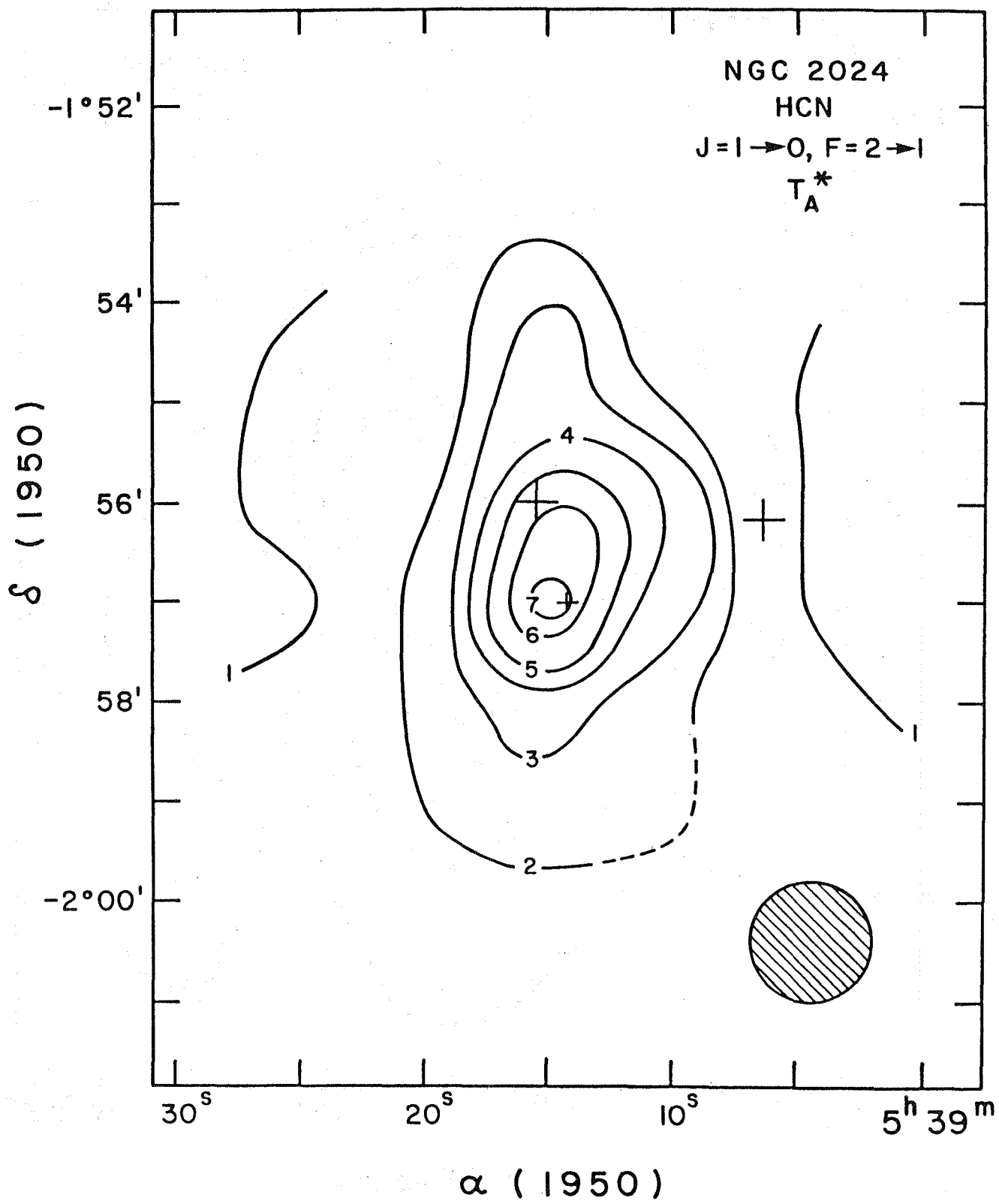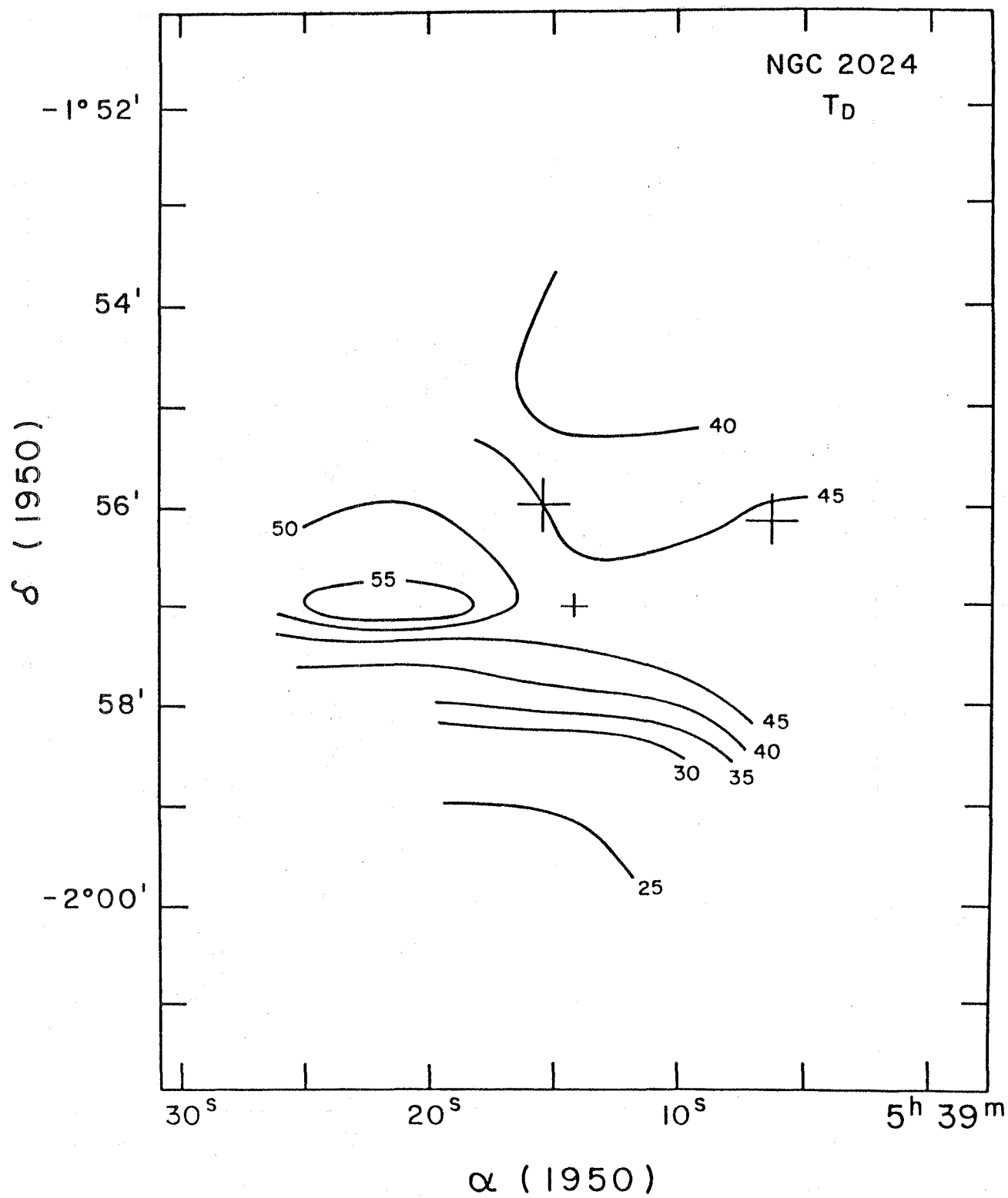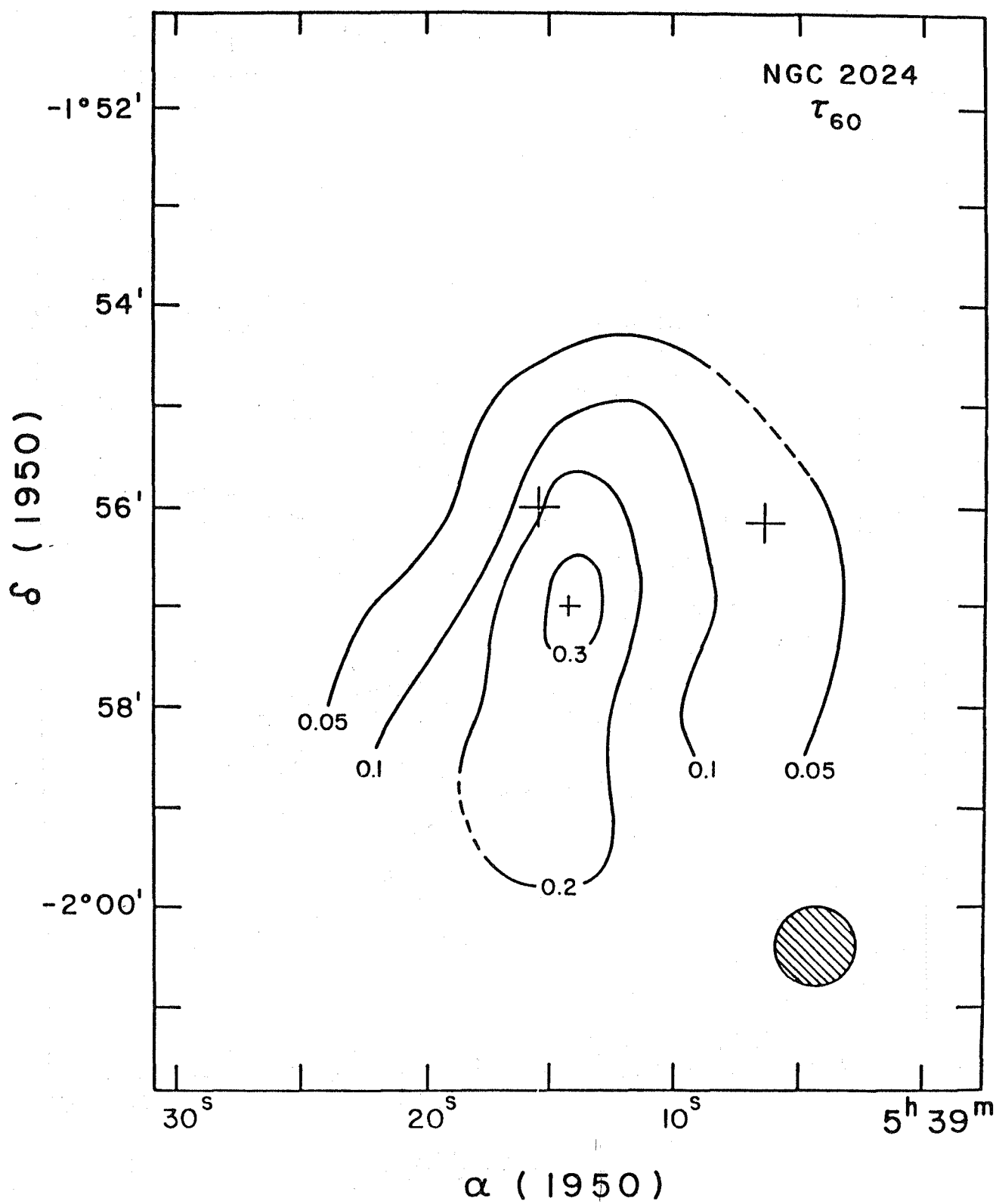
Fig. 8

40

Fig. 9

1. Report No. NASA TM-85954	2. Government Accession No.	3. Recipient's Catalog No.
4. Title and Subtitle NGC 2024: FAR-INFRARED AND RADIO MOLECULAR OBSERVATIONS		5. Report Date May 1984
		6. Performing Organization Code
7. Author(s) Harley A. Thronson, Jr.,* Charles J. Lada,† P. R. Schwartz,‡ Howard A. Smith,‡ J. Smith,*§ W. Glaccum,§ D. A. Harper,§ and R. F. Loewenstein§		8. Performing Organization Report No. A-9764
		10. Work Unit No.
9. Performing Organization Name and Address *Wyoming Infrared Observatory, Univ. of Wyoming, Laramie, WY 82071 †Steward Observatory, Univ. of Arizona, Tucson, AZ 85721 ‡E. O. Hulburt Center for Space Research, Naval Research Laboratory, Washington, DC 20375 §Yerkes Observatory, Univ. of Chicago, Williams Bay, WI 53191		T-5726
		11. Contract or Grant No.
		13. Type of Report and Period Covered Technical Memorandum
12. Sponsoring Agency Name and Address National Aeronautics and Space Administration Washington, DC 20546		
		14. Sponsoring Agency Code 352-02-03

15. Supplementary Notes

Preprint Series #013. Supported by NASA grants. Point of Contact: L. C. Haughney, Ames Research Center, MS 211-12, Moffett Field, CA 94035. (415) 965-5339 or FTS 448-5339

16. Abstract

We present new far-infrared continuum and millimeter-wave molecular observations of NGC 2024. The measurements were obtained at relatively high angular resolution, enabling us to describe the source energetics and mass distribution in greater detail than previously reported. The object appears to be dominated by a dense ridge of material, extended in the north-south direction and centered on the dark lane that is seen in visual photographs. Our maps of the source using the "high-density" molecules CS and HCN confirm this picture and allow us to describe the core structure and molecular abundances. The radio molecular and infrared observations support the idea that an important exciting star in NGC 2024 has yet to be identified and is centered on the dense ridge about 1' south of the bright mid-infrared source IRS 2. The data presented here, along with other observations, allow us to describe a model for the source.

17. Key Words (Suggested by Author(s)) Infrared: Sources Interstellar: Molecules Nebulae: H II region Nebulae: Individual (NGC 2024) Radio sources: General	18. Distribution Statement Unlimited Subject Category - 89

19. Security Classif. (of this report) Unclassified	20. Security Classif. (of this page) Unclassified	21. No. of Pages 43	22. Price* A03

End of Document